

Magnetosphere-ionosphere waves

A. J. B. Russell¹ and A. N. Wright²

Received 22 June 2011; revised 10 October 2011; accepted 7 November 2011; published 5 January 2012.

[1] Self-consistent electrodynamic coupling of the ionosphere and magnetosphere produces waves with clearly defined properties, described here for the first time. Large scale (ideal) disturbances to the equilibrium, for which electron inertia is unimportant, move in the direction of the electric field at a characteristic speed. This may be as fast as several hundred meters per second or approximately half the $\mathbf{E} \times \mathbf{B}$ drift speed. In contrast, narrow scale (strongly inertial) waves are nearly stationary and oscillate at a specific frequency. Estimates of this frequency suggest periods from several tenths of a second to several minutes may be typical. Both the advection speed and frequency of oscillation are derived for a simple model and depend on a combination of ionospheric and magnetospheric parameters. Advection of large scale waves is nonlinear: troughs in E-region number density move faster than crests and this causes waves to break on their trailing edge. Wavebreaking is a very efficient mechanism for producing narrow (inertial) scale waves in the coupled system, readily accessing scales of a few hundred meters in just a few minutes. All magnetosphere-ionosphere waves are damped by recombination in the E-region, suggesting that they are to be best observed at night and in regions of low ionospheric plasma density. Links with observations, previous numerical studies and ionospheric feedback instability are discussed, and we propose key features of experiments that would test the new theory.

Citation: Russell, A. J. B., and A. N. Wright (2012), Magnetosphere-ionosphere waves, *J. Geophys. Res.*, *117*, A01202, doi:10.1029/2011JA016950.

1. Introduction

[2] One of the most fundamental interactions between Earth's magnetosphere and ionosphere is self-consistent electrodynamic coupling. Magnetospheric field-aligned currents (FACs), carried predominantly by the motion of electrons parallel to the magnetic field, can modify the ionosphere by acting there as a source or sink of electrons. Meanwhile, changes to ionospheric conductance (caused, e.g., by changes to ionospheric plasma density) can alter electromagnetic fields in the magnetosphere via the inductive effect of E-region electric currents. When solved self-consistently, with the ionosphere and magnetosphere each responding to their changing partner, the fully coupled system exhibits emergent behavior that includes boundary-waves and efficient multiscale coupling.

[3] Self-consistent electrodynamic magnetosphere-ionosphere (M-I) coupling has previously been studied in the contexts of ionospheric feedback instability (IFI) and the evolution of downward current channels. For example, the studies by Atkinson [1970], Holzer and Sato [1973], Sato [1978], Lysak [1991], and Lysak and Song [2002] (among others) have

shown that narrow-scale perturbations can grow exponentially in a coupled M-I system driven by large-scale background convection, provided that magnetospheric Alfvén waves are partially trapped in some kind of cavity. This effect is known as ionospheric feedback instability and has been proposed as a possible mechanism for the formation of narrow auroral arcs. In a different line of research, Cran-McGreehin *et al.* [2007] have applied self-consistent M-I coupling to the evolution of downward FACs. They showed that strong downward current leads to evacuation of electrons from the E-region and can cause subsequent broadening of the downward FAC. When electron inertia is included in the magnetosphere, this process produces intense field-aligned currents and ionospheric plasma density perturbations at inertial length scales [Streltsov and Lotko, 2004].

[4] Wave-like behavior has been observed in previous M-I coupling studies (such as those referenced above) but it has not been investigated in detail. As a result, no intuitive description of these waves has been previously forthcoming. Here, we address the issue, using a simplified model to focus on local aspects of M-I coupling, and obtaining results that offer new and practical understanding of M-I dynamics.

2. Model

2.1. Local Approximation

[5] Figure 1 illustrates a system composed of a magnetosphere, F-region, E-region and electrically insulating

¹School of Physics and Astronomy, University of Glasgow, Glasgow, UK.

²School of Mathematics and Statistics, University of St Andrews, St Andrews, UK.

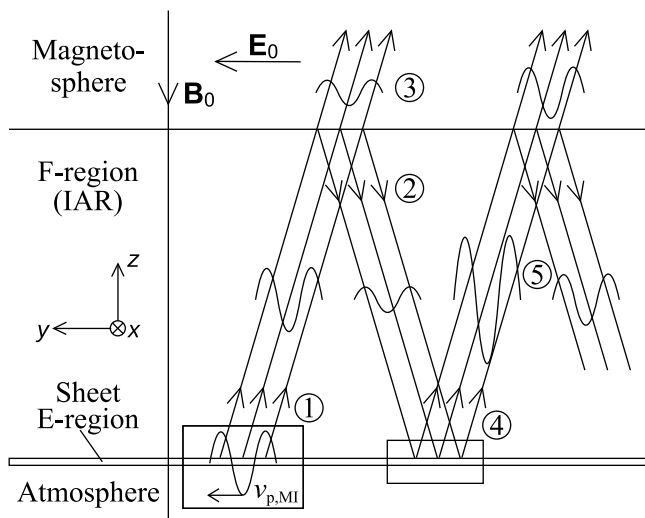


Figure 1. Local interactions and trapping in the ionospheric Alfvén resonator (IAR). At point 1, local interaction between E-region and overlying plasma causes spontaneous radiation of inertial Alfvén waves (IAWs). At point 2, upgoing IAWs are partially reflected from non-uniformities in the F-region to produce downgoing IAWs. At point 3, some part of upgoing IAWs is transmitted, escaping into the magnetosphere. At point 4, local interaction of E-region may cause substantial overreflection of incident IAWs. At point 5, trapping and overreflection may cause a net increase in IAW amplitudes, constituting amplification through ionospheric feedback instability (IFI). Boxes indicate local processes.

atmosphere. Alfvén waves (inertial if small scales are present) propagate in the F-region and magnetosphere and may be partially reflected from non-uniformities. Processes involving the E-region, such as spontaneous emission of Alfvén waves (left-hand box in Figure 1, considered in sections 3–5) or reflection of incident waves (right-hand box in Figure 1, considered in section 6) are dominated by ‘magnetospheric’ conditions in the vicinity of the E-region (i.e. at the base of the F-region). In this respect, these are local processes.

[6] The attributes of local processes involving the E-region are preserved if the non-uniform F-region and magnetosphere are replaced with a uniform plasma. Conceptually, this local approximation is akin to focusing on the local regions indicated by boxes in Figure 1. In the simplified model, upgoing Alfvén escape to infinity, excluding growth of IFI, although the effects of IFI can be approximated by changing the amplitude of an incident wave over time.

[7] Local approximation is advantageous because it produces a mathematically tractable model that can offer new understanding of and insights into self-consistent M-I coupling. A similar local approach has been exploited productively in the past by *Lysak and Song* [2002] to investigate the energization of IFI through overreflection: now we follow a similar vein and examine the dynamics of local M-I coupling in this way. It is anticipated that future studies will explore the modifications that are sure to arise as additional physics is included but we also note that

simple models often prove robust and always provide a useful point of reference.

2.2. Geometry

[8] For this analysis, we have chosen a 2D model in which a thin ‘sheet’ E-region separates a collisionless plasma of uniform number density from an electrically insulating atmosphere. The equilibrium magnetic field is assumed to be vertical and homogeneous, making the model best suited to high magnetic latitudes. Cartesian coordinates (x, y, z) are used where z is ‘up’ and the positive transverse electric field points along the y direction. The remaining coordinate, x , is assumed invariant. Coordinates are indicated in Figure 1.

2.3. Coupling Equations

[9] M-I coupling is described by two equations. First, the effect of magnetospheric field-aligned current on ionospheric electron density is modeled with the E-region electron continuity equation:

$$\frac{\partial n}{\partial t} = \frac{1}{e} \frac{\partial j_z}{\partial z} + \alpha(n_s^2 - n^2), \quad (1)$$

where n is the electron number density, j_z is the vertical (field-aligned) current density in the E-region, e is the fundamental charge, α is the recombination coefficient that we take to be constant and αn_s^2 is a source term representing ionization.

[10] It is convenient to work with the height-integrated form of equation (1). If n is independent of height, then the height integrated electron density is $N = hn$, where h is the thickness of the E-region. Taking $j_z = 0$ at the base of the E-region, integration of (1) gives

$$\frac{\partial N}{\partial t} = \frac{j_z}{e} + \frac{\alpha}{h}(N_s^2 - N^2), \quad (2)$$

where j_z now represents the current at the top of the E-region. The right-hand side of equation (2) is made up of three terms that act as sources or sinks of electrons. Field-aligned currents, carried by the motion of electrons, can both deposit or remove E-region electrons according to the sign of j_z . Here, we assume that precipitating electrons have low energies and do not create additional ionospheric electrons by ionization. The next term, $\alpha N_s^2/h$ is a constant ionization and the final term, $-\alpha N^2/h$ models recombination. In a steady state without FACs, ionization and recombination balance to give $N = N_s$.

[11] M-I coupling is completed by an ionospheric boundary condition imposed at the base of the magnetosphere. Pedersen current in the E-region obeys

$$j_y = \frac{1}{\mu_0} \frac{\partial b_x}{\partial z} = \sigma_P E_y, \quad (3)$$

where σ_P is the Pedersen conductance. Taking $b_x = 0$ at the base of the ionosphere (from 2D geometry and $j_z = 0$ in the atmosphere) and assuming that E_y remains approximately constant over the height of the E-region, integration of (3) over z gives

$$b_x = \mu_0 \Sigma_P E_y \quad (4)$$

at the top of the ionosphere, where Σ_P is the height integrated Pedersen conductance. To a good approximation, Σ_P is proportional to N , allowing us to write

$$\Sigma_P = eM_P N, \quad (5)$$

where M_P is the Pedersen mobility (assumed constant in our model). Putting this into (4), the ionospheric boundary condition is

$$b_x = \mu_0 e M_P N E_y. \quad (6)$$

This is a convenient 2D equivalent of the current closure condition commonly used by other M-I coupling studies, e.g., *Streltsov and Lotko [2004]*.

2.4. Magnetospheric Description

[12] The magnetosphere is modeled as a collisionless plasma dominated by the $\mathbf{j} \times \mathbf{B}$ Lorentz force (gravity and thermal pressure are neglected). Electric and magnetic fields obey Maxwell's equations and we concern ourselves with timescales that are much longer than the plasma oscillation period, making the plasma quasi-neutral. Ohm's law is generalized to include both a transverse electric field due to bulk motion of the plasma and a parallel electric field due to electron inertia.

[13] If magnetic field disturbances, \mathbf{b} , are assumed to have much smaller amplitude than the vertical background magnetic field, \mathbf{B}_0 , then invariance in the x direction allows description of the magnetosphere in terms of linear inertial Alfvén waves (AWs) without coupling to other wave modes.

[14] Inertial AWs are characterized by two wavefields, E_y , and b_x , that satisfy

$$\frac{\partial E_y}{\partial t} = v_A^2 \frac{\partial b_x}{\partial z} \quad (7)$$

and

$$\frac{\partial b_x}{\partial t} - \frac{\partial}{\partial y} \left(\lambda_e^2 \frac{\partial^2 b_x}{\partial y \partial t} \right) = \frac{\partial E_y}{\partial z}. \quad (8)$$

Here,

$$v_A = \frac{B_0}{\sqrt{\mu_0 m^+ n_m}} \quad (9)$$

is the Alfvén speed in the magnetosphere (m^+ is the magnetospheric ion mass and n_m the magnetospheric plasma number density) and

$$\lambda_e = \sqrt{\frac{m^-}{\mu_0 n_m e^2}} \quad (10)$$

is the electron inertial length (m^- is the electron mass). Field-aligned current is given by the z -component of Ampère's law

$$j_z = -\frac{1}{\mu_0} \frac{\partial b_x}{\partial y}, \quad (11)$$

and electron inertia produces a parallel electric field

$$E_z = \mu_0 \lambda_e^2 \frac{\partial j_z}{\partial t}. \quad (12)$$

[15] Examining equation (8), electron inertial effects become significant when length scales perpendicular to the background magnetic field, λ_\perp , are comparable to λ_e . In practice the system is characterized by three regimes: a so-called 'ideal' regime where $\lambda_\perp \gg \lambda_e$ and electron inertia plays a vanishing role; a weakly inertial regime where $\lambda_\perp \approx \lambda_e$ makes electron inertia significant but not dominant; and a strongly inertial regime where $\lambda_\perp \ll \lambda_e$ means electron inertial effects dominate inertial AW behavior.

3. Ideal M-I Waves

3.1. Analytic Results

[16] It is instructive to derive a single governing equation for the coupled M-I system, valid in the ideal (single-fluid MHD) regime of large length scales.

[17] Ideal Alfvén waves are non-dispersive, permitting us to split them into upgoing and downgoing components. This is a valuable tool that has previously been exploited in similar contexts by *Cran-McGreehin et al. [2007]* and *Russell et al. [2010]*.

[18] The downgoing AW component, incident on the ionosphere, has electric and magnetic fields that satisfy

$$E_i = v_A b_i \quad (13)$$

and the upgoing component, reflected from the ionosphere, has fields that satisfy

$$E_r = -v_A b_r. \quad (14)$$

Putting $E_y = E_i + E_r$ and $b_x = b_i + b_r$ into equation (6), some algebra yields

$$b_x = \frac{2QNE_i}{v_A(1+QN)}, \quad (15)$$

where $Q = \mu_0 v_A e M_P$ is a convenient product of constants. Although Q does not have a particular physical significance

$$\Sigma_P / \Sigma_A = (\mu_0 v_A) (e M_P N) = QN \quad (16)$$

is the ratio of the height-integrated Pedersen conductance, $\Sigma_P = e M_P N$, to the ideal Alfvén conductance, $\Sigma_A = 1/(\mu_0 v_A)$. This conductance ratio is an important property of the M-I system.

[19] Next, equations (15) and (11) can be used to write (2) as

$$\frac{\partial N}{\partial t} + \frac{1}{e \mu_0} \frac{\partial}{\partial y} \left(\frac{2QNE_i}{v_A(1+QN)} \right) = \frac{\alpha}{h} (N_s^2 - N^2). \quad (17)$$

The electric field in this equation, $E_i(y, t)$, is assumed to originate from magnetospheric processes far from the ionosphere, e.g. Dungey convection, so it can be treated as a specified quantity. Thus, equation (17) is a single governing equation for a single unknown, $N(y, t)$. An analogous

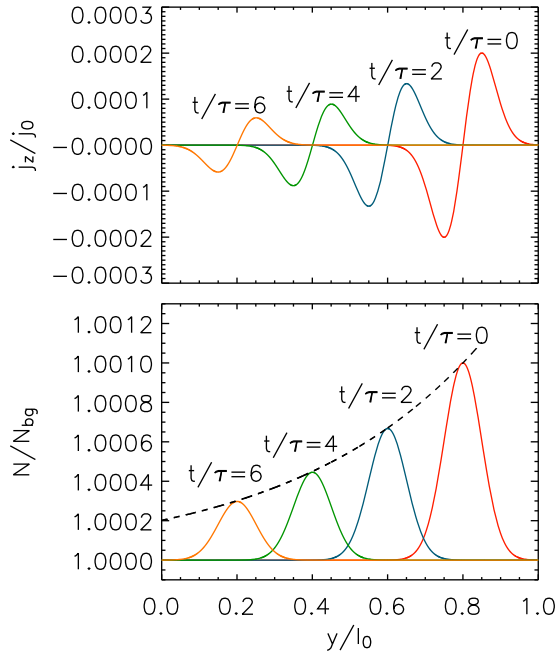


Figure 2. Advection and damping of an ideal M-I wave in the linear regime, demonstrated by computer simulation. M-I waves are coupled phenomena involving (bottom) height-integrated E-region number density and (top) field-aligned current at the base of the magnetosphere. Gradients in N correspond to FACs and this relationship produces advection. The dashed line in Figure 2 (bottom) predicts the peak in N at each location, assuming the wave packet decays exponentially with an e-folding time τ_d while moving in the direction of the electric field at the M-I wave speed v_{MI} . The theory and simulation agree perfectly.

equation has previously been studied by *Cran-McGreehin et al.* [2007] and *Russell et al.* [2010].

[20] The nature of ideal M-I waves is revealed by one further manipulation, that allows novel and intuitive interpretation of large-scale M-I dynamics. Expanding the spatial derivative in (17) and reorganizing,

$$\frac{\partial N}{\partial t} + v_{MI}(N) \frac{\partial N}{\partial y} = F(N), \quad (18)$$

where

$$v_{MI}(N) = \frac{2M_P E_i}{(1 + QN)^2} \quad (19)$$

and

$$F(N) = \frac{\alpha}{h} (N_s^2 - N^2) - \frac{2QN}{e\mu_0(1 + QN)} \frac{\partial}{\partial y} \left(\frac{E_i}{v_A} \right). \quad (20)$$

[21] Equation (18) has the form of a nonlinear advection equation, so structures in N move in the y -direction at a speed v_{MI} as if carried by a flow. Examining equation (19), v_{MI} has the same sign as the incident electric field so ionospheric density structures move in the direction of the

electric field. The speed formula is nonlinear in N . This leads to steepening of waveforms and efficient production of narrow scales, properties that are examined in section 5.

[22] The right hand side of (18) governs changes to density structures as they advect. Physically,

$$F(N) = \frac{\partial N}{\partial t} + v_{MI}(N) \frac{\partial N}{\partial y} = \frac{dN}{dt} \quad (21)$$

is the rate of change of N in an element moving with speed v_{MI} .

[23] The first term on the right hand side of equation (20) captures the effects of recombination and ionization. If E_i/v_A is uniform (the incident wave does not shear the magnetic field, so it does not carry FAC) then $N = N_s$ in equilibrium. Should N be linearly perturbed from N_s (so that $N = N_s + \delta N$ where $\delta N \ll N_s$), then (using $n_s = N_s/h$) the perturbation dies exponentially with an e-folding time

$$\tau_d = 1/(2\alpha n_s). \quad (22)$$

Thus, M-I waves are damped by recombination and ionization.

[24] The second term on the right hand side of equation (20) captures the effect of field-aligned currents in the incident Alfvén wave. At any given location, it is the rate of change of N due to FAC that would occur if N were uniform. For example, if a density structure is advected into a region where the incident Alfvén wave contains downward FAC, N decreases as electrons are removed from the E-region to supply the magnetospheric current.

[25] To briefly recap, E-region density disturbances move in the direction of the horizontal electric field at a speed given by equation (19). They are damped by recombination/background-ionization and are modified by background FACs, both effects being included in the convective derivative (20).

3.2. Simulation of Advection and Damping

[26] The conclusions of section 3.1 are readily confirmed by numerical simulations. This is also an opportunity to see how the ionospheric part of an M-I wave, namely structures in N , interacts with the magnetospheric part, best viewed through j_z at the top of the E-region.

[27] Ideal simulations were performed using a 1D code that solves equation (17) for uniform E_i with periodic boundary conditions in y . This is a modified version of the code described by *Russell et al.* [2010]. Spatial derivatives are approximated using first-order-accurate one-sided finite differences and a first-order-accurate Euler scheme is used for time stepping.

[28] Distances are normalized with respect to the width of the domain, l_0 , N is normalized with respect to N_s , and E_y is normalized with respect to $|E_i|$. This gives a typical speed $v_0 = |E_i|/|B_0|$ (the amplitude of the magnetospheric velocity perturbation caused by the incident Alfvén wave) and a typical timescale $\tau = l_0/v_0$. Current density, j_z , is normalized with respect to $j_0 = \sum_{P0} |E_i|/l_0$ where $\sum_{P0} = eM_P N_s$. (The inertial simulations of sections 4.2 and 5 are normalized to different τ and j_0 .)

[29] Figure 2 shows the evolution of a small-amplitude disturbance in N that initially has the shape of a Gaussian

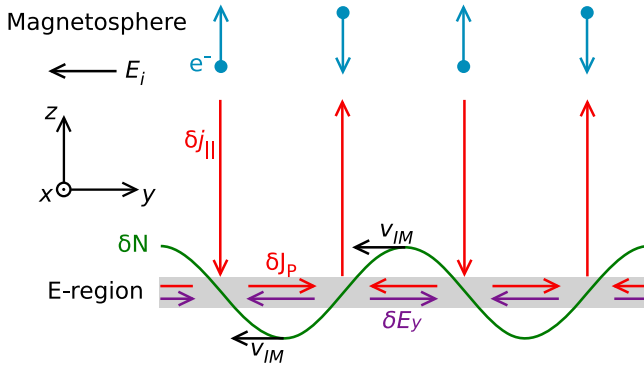


Figure 3. Cartoon of an ideal M-I wave. Gradients in N produce FACs in the magnetosphere by reflection of an incident Alfvén wave. The FACs, in turn, modify N by addition and removal of E-region electrons. The two-way coupling causes advection. A similar cartoon was given by *Miura and Sato* [1980].

wave packet. The small amplitude ensures that the wave is linear; it is not intended to represent the likely amplitude of a physical disturbance. Parameters were chosen to give a normalized advection speed $v_{MI} = -0.1v_0$ in the limit $N \rightarrow N_s$ (the minus sign indicating that the electric field is directed to the left) and a damping time $\tau_d = 5\tau$. Snapshots show the solution at four different times and confirm that the wave packet moves in the direction of the background electric field at the expected speed. The linear wave packet maintains its shape but damps in time. The dashed line in Figure 2 (bottom) shows how the amplitude of N is expected to decay due to recombination as the wave packet moves. The simulation and theory agree perfectly.

[30] M-I waves are a coupled phenomenon with signatures in both the ionosphere and magnetosphere. Indeed, it is the interplay between N and j_z at the base of the magnetosphere that causes advection (discussed in section 3.3). FACs (constituting the magnetospheric part of M-I waves) are carried outwards into the magnetosphere as upgoing Alfvén waves with properties determined the M-I interaction. M-I coupling will, therefore, make itself felt far from the ionosphere.

3.3. Qualitative Description of Advection

[31] Figure 2 shows a relationship between gradients of N (Figure 2, bottom) and FACs in the magnetosphere (Figure 2, top). By adding to this, we can build an intuitive picture of an M-I wave, which is given in cartoon form as Figure 3.

[32] When a uniform incident Alfvén wave reflects from a non-uniform E-region, it can be shown from equation (15) that the total (incident plus reflected) magnetic field perturbation is greatest at maxima in N and least at minima of N . Ampère’s law (11) states that shears in the magnetic field are FACs, so gradients in N correspond to FACs. In the cartoon, $E_i \hat{y}$ is assumed to point to the left, making E_i and b_i negative. This results in upwards FAC where $\partial N / \partial y > 0$, that deposits electrons in the E-region, and downward FAC where $\partial N / \partial y < 0$, that removes electrons from the E-region. The addition and removal of electrons is exactly that needed

to make any waveform move in the direction of the horizontal electric field, advecting at the speed given by equation (19).

[33] An equivalent way of understanding M-I waves is through motion of E-region ions as Pedersen current. Two competing effects determine the Pedersen current. First, reflection of the incident wave from a maximum in N produces a weaker total electric field than reflection from a lesser value of N . Thus, the electric field is reduced at maxima in N compared with at minima in N . On the other hand, an enhancement in N increases ionospheric conductance. The resulting Pedersen current, $J_P = eM_P N E_y$, is slightly enhanced at maxima in N and slightly reduced at minima. Since Pedersen current is carried by the cross-field motion of ions, these changes to J_P can also be viewed as causing the advection of ideal M-I waves. The electron picture and the ion picture do of course fit exactly, because FACs and Pedersen currents form closed current loops, and electron and ion densities match to ensure quasi-neutrality.

4. Inertial M-I Waves

4.1. Analytic Results

[34] When electron inertia is considered for the magnetosphere, Alfvén waves become dispersive at small length scales and an advection equation equivalent to that in section 3.1 no longer exists. In this situation, the most revealing treatment is a linear normal mode analysis, from which a dispersion relation and dispersion diagram can be produced.

[35] The analysis is performed for perturbations from an equilibrium so that

$$N(y, t) = N_0(y) + \delta N(y, t). \quad (23)$$

where $N_0(y)$ is a steady state E-region plasma-density obtained in the presence of some incident Alfvén wave. Reflection of the existing incident Alfvén wave from the perturbed E-region produces perturbed fields at the top of the E-region that can be written as

$$b_x = b_{x0} + \delta b_x, \quad (24)$$

$$E_y = E_{y0} + \delta E_y, \quad (25)$$

where b_{x0} and E_{y0} are the total (incident plus reflected) fields that existed in the steady state.

[36] The dispersion relation assumes that perturbations are linear normal-modes proportional to $\exp(i(\mathbf{k} \cdot \mathbf{r} - \omega t))$, an assumption that is valid provided the wavelength of the normal-mode is much less than the shortest length scale of the steady state and $\delta N \ll N_0$. Normal-mode structure means that derivatives of perturbations simplify to $\partial / \partial y \equiv ik_y$, and $\partial / \partial t \equiv -i\omega$, while $\delta N \ll N_0$ allows products of two or more perturbations to be neglected where they appear in the governing equations. Here, angular frequency, ω , is allowed to be complex but k_y is real.

[37] Substituting equations (23)–(25) into (6) and equating linear terms, the linearized ionospheric boundary condition is

$$\frac{\delta b_x}{b_{x0}} - \frac{\delta E_y}{E_{y0}} = \frac{\delta N}{N_0}. \quad (26)$$

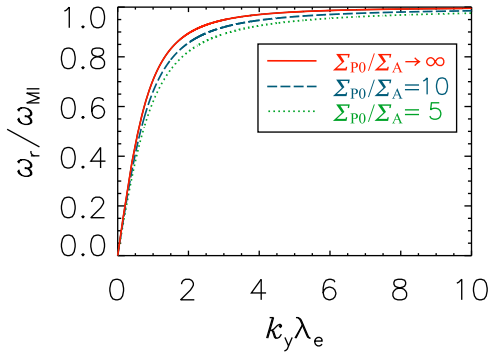


Figure 4. Dispersion diagram for M-I waves showing the effects of electron inertia. The three curves represent different values of Σ_{P0}/Σ_A , showing that frequency at fixed $k_y \lambda_e$ increases slightly with Σ_{P0}/Σ_A . For small $k_y \lambda_e$ (ideal length scales), $\omega_r/k_y = v_{MI}$ is independent of k_y , so density disturbances advect at this speed. For $k_y \lambda_e \gtrsim 2\pi$ (strongly inertial length scales), $\omega_r \rightarrow \omega_{MI}$.

Equation (2) is also linearized. Using equation (11) to replace j_z , taking $\delta N \ll N_0$ and simplifying derivatives, (2) becomes

$$\left(\omega + \frac{2i\alpha N_0}{h}\right)\delta N = \frac{k_y}{e\mu_0}\delta b_x. \quad (27)$$

Equations (26) and (27) are two equations for three perturbations, so a third relation is required to close the system. This comes from the behavior of inertial Alfvén waves in the magnetosphere. For an M-I waves solution, the perturbations δb_x and δE_y form an upgoing inertial Alfvén wave and therefore satisfy

$$\delta E_y = -v_A \sqrt{1 + k_y^2 \lambda_e^2} \delta b_x, \quad (28)$$

where λ_e is the electron inertial length given by (10).

[38] The closed set of linearized equations (26)–(28) is easily solved. Using $b_{x0} = \mu_0 e M_P N_0 E_{y0}$, the dispersion relation for M-I waves is

$$\omega = \frac{k_y M_P E_{y0}}{1 + (\Sigma_{P0}/\Sigma_A) \sqrt{1 + k_y^2 \lambda_e^2}} - i2\alpha n_0. \quad (29)$$

Here, we continue to define $\Sigma_A = 1/(\mu_0 v_A)$ as the ideal Alfvén conductance, making the k_y dependence in (29) fully explicit.

[39] The imaginary part of (29) corresponds to exponential decay with an e-folding time $\tau_d = 1/(2\alpha n_0)$. Interestingly, this damping rate (also seen in the work by *Sato* [1978]) just depends upon n_0 in the ionosphere.

[40] The real part of (29) shows the oscillatory properties of the solution. We take the real part as

$$\omega_r = \omega_{MI} \frac{(\Sigma_{P0}/\Sigma_A) k_y \lambda_e}{1 + (\Sigma_{P0}/\Sigma_A) \sqrt{1 + k_y^2 \lambda_e^2}}, \quad (30)$$

where

$$\omega_{MI} = \frac{M_P E_{y0}}{\lambda_e (\Sigma_{P0}/\Sigma_A)}. \quad (31)$$

The behavior of M-I waves, from the ideal regime to the strongly inertial regime, is revealed by a plot of ω_r/ω_{MI} against $k_y \lambda_e$. This dispersion diagram is given as Figure 4.

[41] Two velocities are important in interpreting the dispersion diagram. At any point on the curve, the gradient of a straight line that also passes through the origin is $v_{p,MI}/(\omega_{MI} \lambda_e)$, where

$$v_{p,MI} = \frac{\omega_r}{k_y} = \frac{M_P E_{y0}}{1 + (\Sigma_{P0}/\Sigma_A) \sqrt{1 + k_y^2 \lambda_e^2}} \quad (32)$$

is the phase velocity. The slope of the curve is $v_{g,MI}/(\omega_{MI} \lambda_e)$, where

$$v_{g,MI} = \frac{\partial \omega_r}{\partial k_y} = M_P E_{y0} \frac{\left(1 + (\Sigma_{P0}/\Sigma_A) / \sqrt{1 + k_y^2 \lambda_e^2}\right)}{\left(1 + (\Sigma_{P0}/\Sigma_A) \sqrt{1 + k_y^2 \lambda_e^2}\right)^2} \quad (33)$$

is the group velocity. Individual peaks or troughs appear to move at the phase velocity, but the group velocity (which may be different) governs the propagation of the disturbance into new areas.

[42] In the limit of large length scales ($k_y \lambda_e \lesssim 1$), group and phase velocities are equal to one another and independent of k_y . Both velocities become the linear version of v_{MI} , obtained by taking $N \rightarrow N_0$ in equation (19). Hence, density structures are advected, recovering the single-fluid MHD results of section 3.1.

[43] The intermediate, weakly inertial regime ($1 \lesssim k_y \lambda_e \lesssim 2\pi$) is characterized by dispersive waves for which $v_{g,MI} < v_{p,MI}$. Phase motion runs ahead of group motion, although both occur in the direction of the electric field. If wave components are present with a range of different length scales, then the narrower components have slower group and phase speeds than their larger scale counterparts.

[44] For strongly inertial length scales ($k_y \lambda_e \gtrsim 2\pi$), the group velocity goes to zero and $\omega_r \approx \omega_{MI}$. In this limit, the density disturbances remain in a fixed location and oscillate with a period that approaches $\tau_{MI} = 2\pi/\omega_{MI}$ from above.

4.2. Simulation of the Strongly Inertial Regime

[45] A simulation confirms that strongly inertial M-I waves are nearly stationary and oscillate with period approaching $\tau_{MI} = 2\pi/\omega_{MI}$ from above. This was performed using a 2D code that solves for magnetospheric fields directly, while solving and enforcing equations (2) and (6) at an ionospheric boundary. The leapfrog-trapezoidal method is used for time stepping (second-order-accurate in time) and spatial derivatives are represented as second-order-accurate centered finite differences. *Russell* [2010] has previously described the code in detail.

[46] For this simulation, distances are normalized by the horizontal width of the domain, labeled l_0 , while N and E_y are normalized by N_0 and $|E_i|$ respectively. Because magnetospheric fields must be solved explicitly, the natural speed to normalize by is the magnetospheric Alfvén speed

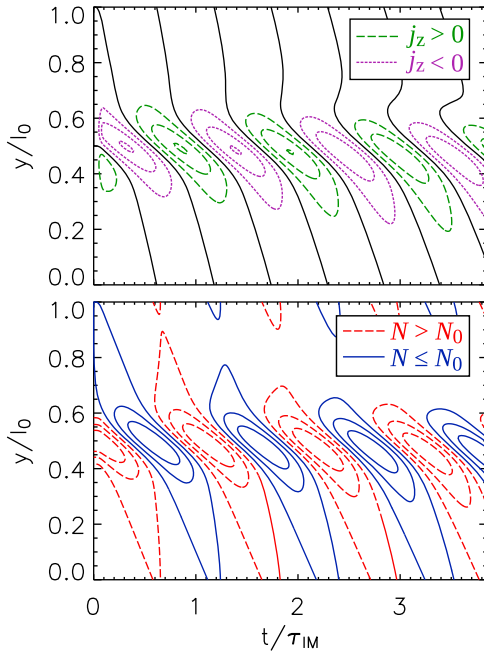


Figure 5. Simulation of a strongly inertial wave packet, the dominant behavior being oscillations with period approaching $\tau_{MI} = 2\pi/\omega_{MI}$ from above. Here, $\lambda_e = 0.5l_0$. Inclined contours reveal a significant phase speed in the direction of the electric field (toward smaller y) but the group speed (again, in the direction of the electric field) is small, especially for the short-wavelength components that constitute the core of the wave packet. Contour spacing is 0.00025 for N/N_0 and 0.0001 for j_z/j_0 .

v_A , giving a typical timescale $\tau = l_0/v_A$. Current density, j_z , is normalized with respect to $j_0 = \Sigma_A |E_i|/l_0$, which differs from the j_0 used to normalize ideal simulations by a factor Σ_A/Σ_{P0} . The simulation domain is sufficiently long in z that artificial reflections do not affect the results.

[47] The electron inertial length was chosen as $\lambda_e = 0.5l_0$, where l_0 is the width of the simulation domain, and the full width at half maximum (FWHM) of the initial Gaussian wave packet was set to $0.118l_0$. This gives a ratio of FWHM to λ_e of 0.235 so the evolution is strongly inertial. The wave packet was initially centered on $y = 0.5l_0$ with a peak of $\delta N = 0.001N_0$ where N_0 is a uniform background value of N . Recombination and ionization were turned off to exclude damping and boundary conditions in y were made periodic. This simulation is driven by an incident Alfvén wave that is uniform apart from a small ramping structure in z at the leading edge. The ramping means that electromagnetic fields at the E-region are initially zero but quickly and smoothly increase to their full values.

[48] Figure 5 shows how the wave packet evolves. The dominant effect is a regular oscillation, with period approaching $\tau_{MI} = 2\pi/\omega_{MI}$ from above, as predicted analytically in section 4.1. Inclined contours show an anticipated phase velocity in the direction of the background electric field, while the location of the wave packet remains reasonably stationary, with only a slight drift in the direction of the electric field. From the slope of Figure 4, group speeds are expected to be small but not quite zero, in keeping with

this observation. Furthermore, long wavelength components are expected to move more rapidly than short wavelengths, a feature that is also plain in Figure 5.

5. Wavebreaking and Production of Narrow Scales

[49] The advection speed for ideal M-I waves, given by equation (19), depends on N such that regions where N is low advect faster than regions where N is high. Thus, troughs in E-region number density inevitably catch up with crests, causing M-I waves to break on their trailing edge. This is of great significance, being a powerful mechanism for the production of narrow spatial scales from large spatial scales.

[50] If the entire wavebreaking process is modeled under the assumption of an ideal magnetosphere, then a large-amplitude wave packet (e.g. with $\delta N = 0.2N_0$) rapidly steepens to form a discontinuity in N at its trailing edge. A discontinuity thus formed moves in the direction of the electric field and is accompanied by a current sheet in the magnetosphere. This type of behavior has previously been seen in the self-consistent M-I coupling simulations of *Cran-McGreehin et al.* [2007].

[51] By integrating equation (18) over a small interval in y around a discontinuity, in the frame of the discontinuity, and performing a little algebra, it is possible to show that such a discontinuity moves at a speed

$$U = \text{sign}(E_i) \sqrt{v_{MI}^+ v_{MI}^-}, \quad (34)$$

where v_{MI}^+ and v_{MI}^- are the M-I wave speed evaluated immediately to the left and right of the discontinuity. This result has been confirmed by simulation.

[52] In the ideal model, wavebreaking quickly collapses the shortest length scale to zero. In reality, new physics becomes important as the length scale converges to zero and this limits the length scales achieved. Therefore, the system follows an ideal evolution and steepens until small scales make electron inertial effects significant.

[53] The complete development of wavebreaking, including the effects of electron inertia, is best illustrated by computer simulation. Our inertial code was used for this purpose, performing a simulation with the electron inertial length set to $\lambda_e = 0.01l_0$ and the initial condition in N being a Gaussian wave packet with a FWHM of $0.118l_0$ and amplitude $\delta N = 0.2N_0$. This combination of length scales allows the wave packet to exist in the ideal regime for a time before wavebreaking makes electron inertial effects significant. The system was driven with a uniform E_i (after an initial ramping transient), recombination and ionization were switched off to exclude damping, and parameters were chosen so that the background advection speed (v_{MI} evaluated for $N = N_0$) is $-0.1v_A$. (As discussed above, the peak in N moves slower than this.)

[54] Figure 6 (bottom) shows evolution of N . At early times (between the first two snapshots), electron inertial effects are negligible, so the wave packet is governed by ideal advection and moves in the direction of the electric field at $v_{MI}(N)$ (left in this simulation). During this time, the trailing edge of the wave packet steepens while the gradient of the leading edge becomes more gentle: this is expected

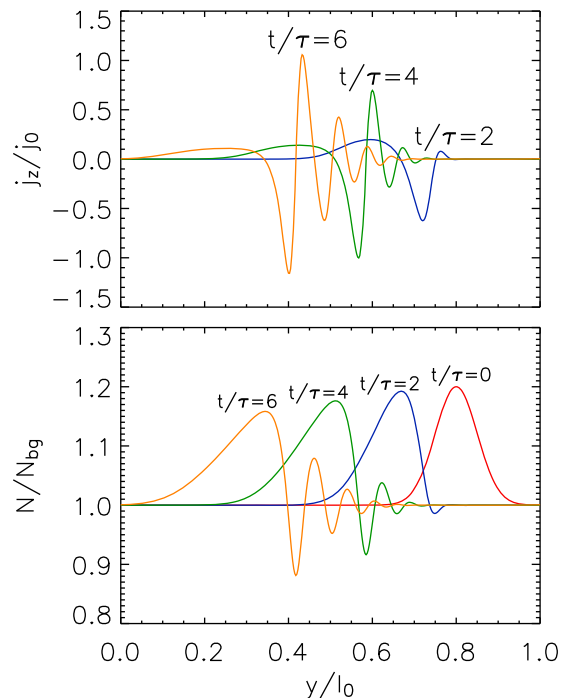


Figure 6. Inertial simulation showing wavebreaking of an M-I wave with powerful production of narrow (inertial) scales and multiple FACs. (bottom) Nonlinear advection of a wave packet in E-region number density: differences in the advection speed steepen the trailing edge of the wave packet until inertial scales are reached. Once electron inertia becomes significant, an undershoot develops behind the main wave packet, later becoming a long train of undershoots and overshoots. (top) The steep gradients in N produce intense, narrow FACs at the base of the magnetosphere, driving upgoing inertial Alfvén waves that carry M-I wave signatures far from the ionosphere.

because the advection speed is lowest at the peak in N . Similar steepening was seen in nonlinear simulations of ionospheric feedback instability by *Lysak and Song* [2002]. This behavior can now be identified with nonlinear advection of M-I waves.

[55] As the trailing edge of the wave packet steepens, electron inertial effects becomes significant, their first signature being an undershoot behind the steepened trailing edge, apparent by $t/\tau = 2$. In time, this feature becomes increasingly pronounced and a long train of undershoots and overshoots develops behind the main wave packet. A close look at the oscillatory structure reveals wavelengths of approximately $2\pi\lambda_e$, the wavelength diminishing with distance behind the large scale wave packet.

[56] Figure 6 (top) shows field-aligned current at the base of the magnetosphere, one of the magnetospheric signatures of the wave. Data are not plotted at $t/\tau = 0$ since the incident Alfvén wave used to drive the simulation is ramped, giving $j_z = 0$ at the base of the magnetosphere at $t/\tau = 0$. At early times, reflection of the incident Alfvén wave from the E-region creates two broad channels of field-aligned current that cause advection of the wave packet as described in

section 3.3. Nonlinear advection of N means that the leading edge of the wave packet becomes more gentle in N , causing the leading FAC to spread out and weaken in current density. The trailing FAC, in contrast, narrows and increases its current density as the trailing edge of the wave packet steepens in N . At later times, narrow scale variations in N translate to steep gradients in ionospheric reflectivity producing multiple intense FACs behind the trailing edge of the wave packet. All FACs in this simulation take the form of upgoing inertial Alfvén waves, that propagate out into the magnetosphere. Therefore, wavebreaking of M-I waves produces narrow scale waves and intense FACs, both near and far from the ionospheric boundary.

[57] The origin of the small-scale, inertial waves can be understood by reference to nonlinear advection of large-scale waves at speed $v_M(N)$, and to the dispersion diagram for linear inertial M-I waves (Figure 4). Initially almost all of the wave power is at wavelengths much larger than the electron inertial length, so waveforms advect in the ideal limit: this causes steepening at the trailing-edge, which transfers power to smaller wavelengths at the expense of larger wavelengths. Subsequently, electron inertial scales become present with slowly growing amplitudes. The evolution of the inertial component appears to be dominated by group and phase velocities very similar to those found for decoupled linear normal modes by dispersion analysis. These speeds are less than the ideal advection speed, so, as power is transferred to inertial wavelengths, the corresponding features fall behind the main wave packet, where they form a trailing oscillatory structure. Analogous behavior occurs in other nonlinear systems with a source of dispersion, for example in viscous shocks (*A. W. Hood, Oscillatory structure in viscous shocks, private communication, 2010*) and collisionless plasma shocks [*Ofman et al., 2009*].

[58] The wavelength of the narrow scale waves is defined by the scale at which dispersive effects noticeably reduce the normal-mode group speed below the ideal advection speed, allowing separation from the main wave packet. By referring to the dispersion diagram (Figure 4), one can estimate this scale as $k_y\lambda_e \approx 1$ implies $\lambda_\perp \approx 2\pi\lambda_e$, in good agreement with the wavelength obtained in the simulation. Further along the wave train (away from the main wave packet) the length scale becomes smaller because the smallest wavelengths (largest k_y) have the smallest group velocities and therefore become most separated from the main wave packet. Since they typically have a smaller amplitude than the main wave packet, the trailing features are freed from the nonlinear cascade to ever smaller wavelengths and significant power does not reach wavelengths much below the electron inertial length.

6. M-I Waves, Overreflection, and IFI

[59] Ionospheric feedback instability (IFI) is a process that amplifies electrodynamic perturbations in a self-consistently coupled M-I system [*Atkinson, 1970; Holzer and Sato, 1973; Sato, 1978; Lysak, 1991; Lysak and Song, 2002*]. It occurs because a downgoing AW perturbation, incident on the E-region, can reflect from the E-region to produce an upgoing AW perturbation of significantly larger amplitude, a

phenomenon described as overreflection [Mann *et al.*, 1999; Lysak and Song, 2002].

[60] Overreflection of downgoing AWs at the E-region energizes the IFI, but reflection of upgoing AWs also plays a role in its development. Upgoing AWs can be reflected, perhaps partially, either from the steep gradient in Alfvén speed at the base of the magnetosphere known as the ionospheric Alfvén resonator (IAR), or from a conjugate ionosphere if traveling along closed field lines. A sequence of reflections may produce a net amplification of AW perturbations (along with corresponding perturbations of the E-region), causing them to grow exponentially until the instability saturates. This process is not unlike amplification of light in a laser: here, a cavity is formed by trapping between the E-region and Alfvén speed gradient or conjugate ionosphere and trapped waves are repeatedly amplified by overreflection from the E-region. In the M-I case, the free energy needed to amplify trapped waves comes from a reduction in background Joule heating of the ionosphere (for a discussion of energetics see Lysak and Song [2002]).

[61] The process of overreflection is a local phenomenon [Mills and Wright, 1999] that, in this case, occurs at the magnetosphere-ionosphere interface and can be characterized through the equations presented in this paper (Figure 1). Overreflection energizes the IFI, and establishing a link between IFI, overreflection and M-I waves can provide a deeper or alternative understanding of each. In particular, the convenient formulas of M-I waves can be exploited. Such an approach is encouraged by the observation that M-I waves, representing spontaneous emission of upgoing inertial AWs, can be viewed as ‘infinite overreflection of a zero-amplitude incident wave’.

6.1. Reflection Analysis

[62] The overreflection problem is characterized by a reflection coefficient, obtained from linear normal-mode analysis. Initial steps are the same as those used in section 4.1 to obtain the M-I wave dispersion relation. Functions N_0 , b_{x0} and E_{y0} are introduced to represent the steady state and these are perturbed to produce equations (23)–(25). Perturbations are described as superpositions of linear normal modes and $\delta N \ll N_0$ is assumed. We therefore solve equations (26) and (27).

[63] This time, δE_y and δb_x are regarded as superpositions of incident (downgoing) and reflected (upgoing) perturbations. Writing $\delta E_y = \delta E_i + \delta E_r$, it is convenient to introduce a reflection coefficient

$$r = \frac{\delta E_r}{\delta E_i} \quad (35)$$

so that

$$\delta E_y = \delta E_i(1 + r). \quad (36)$$

In general, r is complex: its modulus, $|r|$, is the ratio of the amplitude of the upgoing perturbation to the amplitude of the downgoing perturbation; its argument is the phase difference between these components.

[64] A third governing equation, relating δE_y and δb_x and closing the system of equations, comes from the properties

of inertial AWs. Incident and reflected inertial AW perturbations respectively obey

$$\delta E_i = v_A \sqrt{1 + k_y^2 \lambda_e^2} \delta b_i, \quad (37)$$

$$\delta E_r = -v_A \sqrt{1 + k_y^2 \lambda_e^2} \delta b_r. \quad (38)$$

It follows that

$$\delta b_x = \delta b_i(1 - r) \quad (39)$$

and then

$$\delta E_y = \frac{(1 + r)}{(1 - r)} v_A \sqrt{1 + k_y^2 \lambda_e^2} \delta b_x. \quad (40)$$

Equation (40) relates δb_x and δE_y , completing our system of equations.

[65] We now have three equations between which to eliminate δN , δE_y and δb_x , solving for r . Eliminating δE_y between equations (40) and (26),

$$\delta N = \frac{\delta b_x}{\mu_0 e M_P E_{y0}} \left(1 - \frac{\Sigma_{P0}}{\Sigma_A} \sqrt{1 + k_y^2 \lambda_e^2} \frac{(1 + r)}{(1 - r)} \right). \quad (41)$$

Substituting for δN with equation (27) and canceling δb_x ,

$$\frac{(1 + r)}{(1 - r)} = \frac{1}{(\Sigma_{P0}/\Sigma_A) \sqrt{1 + k_y^2 \lambda_e^2}} \left(1 - \frac{k_y M_P E_{y0}}{\omega_r (1 + ic)} \right) \quad (42)$$

where $\omega = \omega_r + i\omega_i$ has been expanded into its real and imaginary parts, and

$$c = \frac{(\omega_i + 2\alpha N_0/h)}{\omega_r}. \quad (43)$$

The introduction of c is mathematically useful because it gathers imaginary terms together. Its physical significance will be discussed in section 6.2.

[66] Some further algebra rearranges equation (42) for r . One convenient form is

$$r = \frac{(1 + c^2)r_0 \tilde{v} - 1 + ic}{(1 + c^2)\tilde{v} - 1 + ic} \quad (44)$$

where

$$r_0 = \frac{1 - (\Sigma_{P0}/\Sigma_A) \sqrt{1 + k_y^2 \lambda_e^2}}{1 + (\Sigma_{P0}/\Sigma_A) \sqrt{1 + k_y^2 \lambda_e^2}} \quad (45)$$

and

$$\tilde{v} = \frac{\omega_r/k_y}{M_P E_{y0} / \left(1 + (\Sigma_{P0}/\Sigma_A) \sqrt{1 + k_y^2 \lambda_e^2} \right)} = \frac{v_{p,y}}{v_{p,MI}} \quad (46)$$

is the ratio of the wave’s phase speed in y , $v_{p,y} = \omega_r/k_y$, to the M-I wave phase-speed defined by equation (32).

[67] The argument of (the complex quantity) r is useful since it is the phase difference between incident and

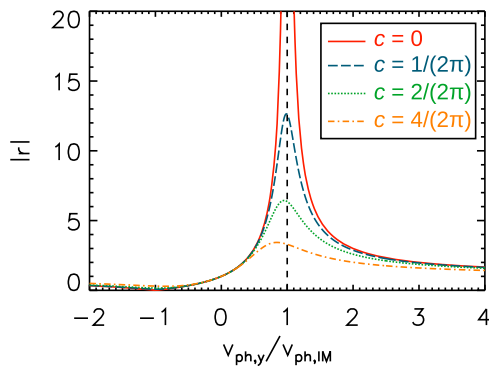


Figure 7. Amplitude of the reflection coefficient plotted for several values of c and using $r_0 = -1$. The peak of r always occurs close to $v_{p,y}/v_{p,MI} = 1$ where the incident inertial AW's phase speed closely matches the phase speed of an M-I wave with the same horizontal length scale. The solution for $c = 0$ is singular at $v_{p,y}/v_{p,MI} = 1$; this represents spontaneous emission of an upgoing inertial AW and corresponds to the M-I wave solution.

reflected waves, but we shall not discuss it further here. We will instead focus on $|r|$ which relates the amplitudes of the incident and reflected waves. This is easily evaluated from equation (44), being

$$|r| = \sqrt{\frac{(1+c^2)r_0^2\tilde{\nu}^2 - 2r_0\tilde{\nu} + 1}{(1+c^2)\tilde{\nu}^2 - 2\tilde{\nu} + 1}}. \quad (47)$$

6.2. Interpretation

[68] Inspection of equation (47), shows that $|r|$ is singular where $\tilde{\nu} = 1$ and $c = 0$. This corresponds to spontaneous emission of an upgoing inertial AW from the ionospheric boundary and is the M-I wave solution. The condition $c = 0$ requires that $\omega_i = -2\alpha N_0/h$, by (43). Therefore, the M-I wave solution decays with an e-folding time $\tau_d = 1/(2\alpha n_0)$, in agreement with the damping theory of section 4.1.

[69] There are an important family of steady solutions that neither grow nor decay, having $\omega_i = 0$. In this situation, equation (43) becomes

$$c = \frac{2\alpha n_0}{\omega_r} = \frac{\tau_{wave}}{2\pi\tau_d} \quad (48)$$

where $\tau_{wave} = 2\pi/\omega_r$ is the period of the wave. Therefore, c is small when the ionospheric damping time (due to recombination and ionization in the E-region) is long compared to the wave period. By requiring that $c \neq 0$, ionospheric damping removes the singularity from $|r|$. Nonetheless, $|r|$ can still reach a considerable maximum value.

[70] Figure 7 plots $|r|$ against $\tilde{\nu} = v_{p,y}/v_{p,MI}$ for several values of c and with $r_0 = -1$. The peak of $|r|$ always occurs close to $\tilde{\nu} = 1$ and represents significant overreflection for all but the most heavily damped (low frequency) waves; as an example, for a steady solution with $\tau_{wave} = \tau_d$ (for which $c = 1/(2\pi)$), the maximum value of $|r|$ is 12.6 and this is

obtained at $\tilde{\nu} = 0.988$. Higher frequency solutions have even greater maximum $|r|$ attained with $\tilde{\nu}$ closer to 1.

[71] Behavior for $\tilde{\nu}$ far from the resonance at $\tilde{\nu} \approx 1$ is revealed by applying the limit $\tilde{\nu} \rightarrow \pm\infty$ to equation (47). This gives $|r| \rightarrow |r_0|$ as $\tilde{\nu} \rightarrow \pm\infty$. We conclude that incident waves whose phase speed is a poor match for $v_{p,MI}$ are reflected as though from a passive ionosphere, with $r = r_0$.

[72] IFI can develop if upgoing waves, produced by overreflection from the E-region, are partially reflected in the IAR to produce secondary downgoing waves. If successive cycles of overreflection from the E-region and partial reflection in the IAR produce an overall increase wave amplitudes then IFI develops. Since the maximum of $|r|$ is typically large, the IAR need only have a small trapping efficiency for waves to become unstable. Both overreflection and trapping determine the properties of unstable modes: overreflection will favor instability of waves whose phase-speed is a close match to the phase-speed of an M-I wave, and constructive interference in the IAR will favor waves of particular frequencies. A quickly growing spatial scale will then follow from $k_y = \omega_{IAR}/v_{p,MI}$ as a consequence of M-I wave and IAR properties.

[73] This analysis provides a simple interpretation of the overreflection condition: Alfvén waves incident on an active ionosphere are greatly overreflected when their phase speed matches the phase speed of an M-I wave with the same horizontal length scale. This is true even if the wave period is several ionospheric damping times, although the greatest overreflection is obtained when the wave period is much shorter than the damping time. The strength of the overreflection means that the trapping requirement for M-I waves to become unstable to IFI is small: only a small percentage of each upgoing inertial AW need be reflected back to the E-region to establish the cycle of amplification. The facts that waves can be overreflected from the ionosphere, that this lies at the heart of IFI and that phase speed affects the susceptibility of a wave to IFI were all known previously [e.g., *Lysak and Song, 2002*]. The real importance of linking overreflection to M-I waves is provision of an interpretive framework that explains the significance of the resonance, identifies the source of the favored phase speed and gives useful formulas. Future work is needed to investigate the time evolution of partially trapped waves in the combined context of M-I waves and IFI.

7. Behavior for a 2D Sheet E-Region

[74] The original M-I waves perspective presented in this paper offers fresh insight into M-I coupling. The approach is both novel and powerful, but it is also built on a tested body of M-I physics shared with the extensively studied subject of ionospheric feedback instability (IFI). Commonalities between these topics are important, not only because M-I waves provide new insight into IFI, but also because existing IFI results can be used to accelerate future development of M-I wave theory.

[75] As an example of the opportunity for rapid development, existing IFI results provide a shortcut to the likely behavior of M-I waves for a 2D sheet E-region. A full treatment is harder for a 2D E-region, partly because the loss of invariance couples Alfvén waves to fast compressional modes. Nonetheless, IFI studies, starting with *Sato [1978]*,

have already derived linear normal-mode dispersion relations for coupled M-I systems and some of the later generalizations of these studies include both a 2D sheet E-region and the effects of electron inertia. The M-I wave viewpoint suggests we look for advection and oscillation at a characteristic frequency. Then, by applying appropriate limits (and algebra) to IFI results, we can generalize our previous M-I wave dispersion relation (29).

[76] Taking equation (11) from *Lysak and Song* [2002], removing the effects of magnetospheric trapping (by setting their magnetospheric reflection coefficient to zero) and performing a little algebra, we obtain the general dispersion relation for 2D M-I waves:

$$\omega = \mathbf{k}_\perp \cdot \mathbf{v}_\perp - \frac{i}{\tau_d}. \quad (49)$$

Here \mathbf{v}_\perp has the form of a phase velocity and it is given by

$$\mathbf{v}_\perp = \frac{\gamma M_P |\mathbf{E}_\perp|}{1 + \sqrt{1 + k_\perp^2 \lambda_e^2 (\Sigma_P / \Sigma_A)}} \hat{\mathbf{E}}_\perp + \left(\frac{|\mathbf{E}_\perp|}{|\mathbf{B}_0|} - \frac{\gamma M_H |\mathbf{E}_\perp|}{1 + \sqrt{1 + k_\perp^2 \lambda_e^2 (\Sigma_P / \Sigma_A)}} \right) \hat{\mathbf{E}}_\perp \times \hat{\mathbf{B}}_0, \quad (50)$$

where vectors with a hat denote unit vectors, M_H is the Hall mobility and γ is a factor that gives the number of electrons produced in the E-region for every precipitating electron ($\gamma = 1$ if FACs are carried by low-energy electrons as previously assumed).

[77] In the ideal limit, $k_\perp^2 \lambda_e^2 \ll 1$ making \mathbf{v}_\perp independent of \mathbf{k}_\perp ; hence ideal M-I waves are non-dispersive. As in the 1D case, 2D M-I waves advect in the direction of the electric field at speed

$$\mathbf{v}_\perp \cdot \hat{\mathbf{E}}_\perp = \frac{\gamma M_P |\mathbf{E}_\perp|}{1 + \Sigma_P / \Sigma_A}, \quad (51)$$

which is equal to v_{MI} for $\gamma = 1$. (Waveforms move faster for greater γ because a given j_z in the magnetosphere effects changes in the E-region more rapidly.)

[78] The new behavior that arises in 2D is a component of advection in the $\mathbf{E}_\perp \times \mathbf{B}_0$ direction. This has a speed

$$\mathbf{v}_\perp \cdot (\hat{\mathbf{E}}_\perp \times \hat{\mathbf{B}}_0) = \frac{|\mathbf{E}_\perp|}{|\mathbf{B}_0|} - \frac{\gamma M_H |\mathbf{E}_\perp|}{1 + \Sigma_P / \Sigma_A}. \quad (52)$$

The first term on the right-hand side of (52) is the $\mathbf{E} \times \mathbf{B}$ drift speed. The second term is similar to v_{MI} in 1D but with M_H taking the place of M_P on the numerator. Therefore, advection not only means that ideal M-I waves move in the direction of the electric field; it also opposes their $\mathbf{E} \times \mathbf{B}$ drift.

[79] In the strongly inertial limit, $k_\perp^2 \lambda_e^2 \gg 1$ and the real part of equation (49) can be written as

$$(\omega_r - \mathbf{k}_\perp \cdot \mathbf{v}_E) = \omega_P \hat{\mathbf{k}}_\perp \cdot \hat{\mathbf{E}}_\perp - \omega_H \hat{\mathbf{k}}_\perp \cdot (\hat{\mathbf{E}} \times \hat{\mathbf{B}}_0), \quad (53)$$

where $\mathbf{v}_E = \mathbf{E}_\perp \times \mathbf{B}_0 / |\mathbf{B}_0|^2$ is the $\mathbf{E} \times \mathbf{B}$ drift velocity,

$$\omega_P = \frac{\gamma M_P |\mathbf{E}_\perp|}{\lambda_e \Sigma_P / \Sigma_A} \quad (54)$$

and

$$\omega_H = \frac{\gamma M_H |\mathbf{E}_\perp|}{\lambda_e \Sigma_P / \Sigma_A}. \quad (55)$$

[80] Two processes are involved in 2D strongly inertial behavior: oscillation at a characteristic frequency and $\mathbf{E} \times \mathbf{B}$ drift. The frequency of oscillation depends on the orientation of $\hat{\mathbf{k}}_\perp$ with respect to $\hat{\mathbf{E}}_\perp$. When \mathbf{k}_\perp and \mathbf{E}_\perp are parallel, $\omega_r = \omega_P$, recovering the characteristic frequency found in 1D. When \mathbf{k}_\perp and \mathbf{E}_\perp are perpendicular, $(\omega_r - \hat{\mathbf{k}}_\perp \cdot \mathbf{v}_E) = -\omega_H$: these M-I waves have a characteristic frequency in which M_H takes the role previously played by M_P and they oscillate at this frequency while carried along by their $\mathbf{E} \times \mathbf{B}$ drift. Most generally, the characteristic oscillation for strongly inertial M-I waves in a 2D sheet E-region takes place at a weighted sum of ω_P and ω_H , the weighting determined by the direction of $\hat{\mathbf{k}}_\perp$ relative to $\hat{\mathbf{E}}_\perp$.

[81] The combination of M-I waves concepts and existing IFI results has extended the M-I waves concepts of advection (in the ideal limit) and characteristic frequency (for the strongly inertial limit) to a 2D sheet E-region, with minimal effort. Now that we have a basis for extending M-I wave concepts to 2D, a fuller investigation should be performed to verify the predictions of the dispersion relation.

8. Discussion

8.1. Useful Expressions and Typical Values

[82] Of the results presented in this paper, three quantities are particularly useful: the advection speed for ideal M-I waves, the oscillation frequency for strongly inertial M-I waves, and the decay time due to recombination and ionization. Because of the importance of these quantities, it is worth listing some of the formulas available for them and estimating their typical values.

8.1.1. Advection Speed for Ideal M-I Waves

[83] The ideal advection speed for M-I waves is given by equation (19) and can be written in terms of any one of the total/incident electric/magnetic field perturbations. The following forms are readily obtained:

$$v_{MI} = \frac{M_P E_y}{(1 + \Sigma_P / \Sigma_A)} \quad (56)$$

$$= \frac{M_P b_x}{\mu_0 \Sigma_P (1 + \Sigma_P / \Sigma_A)} \quad (57)$$

$$= \frac{2 M_P E_i}{(1 + \Sigma_P / \Sigma_A)^2} \quad (58)$$

$$= \frac{2 M_P b_i}{\mu_0 \Sigma_A (1 + \Sigma_P / \Sigma_A)^2}. \quad (59)$$

Of these, the form giving v_{MI} from the total electric field and conductances is perhaps the most convenient.

[84] To estimate v_{MI} for active conditions, we might consider $M_P \approx 10^4 \text{ m}^2 \text{ s}^{-1} \text{ V}^{-1}$, $E_y \approx 0.1 \text{ V m}^{-1}$ and $\Sigma_P / \Sigma_A \approx 5$. Putting these into equation (56) gives a typical advection

speed of 170 ms^{-1} . This could be increased significantly by E-region depletion which decreases the value of Σ_P/Σ_A on the denominator of (56).

[85] The advection speed is given context by the $\mathbf{E} \times \mathbf{B}$ drift speed, $v_E \approx E_y/B_0$. Comparing these speeds,

$$\frac{v_{MI}}{v_E} = \frac{B_0 M_P}{(1 + \Sigma_P/\Sigma_A)}. \quad (60)$$

Substituting for M_P and assuming $B_0 \approx 5 \times 10^{-5} \text{ T}$,

$$\frac{v_{MI}}{v_E} \approx \frac{0.5}{1 + \Sigma_P/\Sigma_A}. \quad (61)$$

For an undepleted ionosphere, v_{MI} is likely to be significantly smaller than v_E ; for example, putting $\Sigma_P/\Sigma_A \gtrsim 5$ into (61) gives $v_{MI}/v_E \lesssim 0.08$. In an E-region density cavity, however, it is possible to have $\Sigma_P/\Sigma_A \ll 1$, so that $v_{MI}/v_E \approx 0.5$ (for the values of M_P and B_0 assumed above). Thus, v_{MI} can be a significant fraction of v_E .

8.1.2. Frequency Limit for Inertial M-I Waves

[86] Disturbances with length scales less than the electron inertial length in the low altitude magnetosphere, oscillate with an angular frequency just below the characteristic limit ω_{MI} , given by equation (31). This can be written in terms of any one of the total-background/incident electric/magnetic field perturbations, yielding the following formulas:

$$\omega_{MI} = \frac{M_P E_{y0}}{\lambda_e (\Sigma_{P0}/\Sigma_A)} \quad (62)$$

$$= \frac{M_P b_{x0}}{\lambda_e \mu_0 \Sigma_{P0} (\Sigma_{P0}/\Sigma_A)} \quad (63)$$

$$= \frac{2M_P E_i}{\lambda_e (\Sigma_{P0}/\Sigma_A) (1 + \Sigma_{P0}/\Sigma_A)} \quad (64)$$

$$= \frac{2M_P b_i}{\lambda_e \mu_0 \Sigma_{P0} (1 + \Sigma_{P0}/\Sigma_A)}. \quad (65)$$

In these formulas for ω_{MI} , E_{y0} , b_{x0} and Σ_{P0} refer to equilibrium (unperturbed) values. Also, the expressions involving incident field perturbations assume that the equilibrium solution is large scale and can therefore be described in terms of an ideal incident Alfvén wave (although the reflected wave may have inertial scales present).

[87] Before estimating ω_{MI} we must first use equation (10) to estimate the electron inertial length in the magnetosphere. Since M-I waves are an interaction between the magnetosphere and the E-region, it is likely that conditions just above the E-region, at the bottom of the F-region, determine the value of ω_{MI} . The chosen value of n_m depends (primarily) on the time of day but an approximate range from $5 \times 10^8 \text{ m}^{-3}$ (night) to 10^{11} m^{-3} (day) is reasonable for polar latitudes [Bilitza, 2001]. With this range for n_m , equation (10) gives λ_e between 17 m (day) and 240 m (night).

[88] Assuming $M_P = 10^4 \text{ m}^2 \text{ s}^{-1} \text{ V}^{-1}$, total $E_{y0} \approx 0.1 \text{ V m}^{-1}$, $\Sigma_P/\Sigma_A \approx 5$ and taking $\lambda_e \approx 170 \text{ m}$, the appropriate formula (62) gives $\omega_{MI} \approx 1.2 \text{ rads}^{-1}$. This corresponds to a period of

approximately 5 s. Changes in the electric field, ratio of conductances and λ_e will all cause variation in this oscillation period, but a range from a few tenths of a second to several minutes appears reasonable.

8.1.3. Lifetime

[89] M-I waves are damped by recombination and ionization acting in the E-region. This damping is described by equation (22), small perturbations decaying exponentially with an e-folding time $\tau_d = 1/(2\alpha n_0)$. The value of τ_d varies substantially depending on which value is chosen for the background (unperturbed) E-region number density, n_0 . If τ_d is calculated using $\alpha \approx 3 \times 10^{-13} \text{ m}^3 \text{ s}^{-1}$ and a typical daytime number density of $n_0 \approx 10^{11} \text{ m}^{-3}$ then the result is $\tau_d \approx 17 \text{ s}$. This suggests that daytime M-I waves are generally short-lived. Lifetimes increase significantly, however, for activity at night and in E-region density cavities. If n_0 decreases to 1% of the value previously assumed (not unreasonable for an E-region density cavity in the nightside ionosphere) then the lifetime of M-I waves may become as large as $\tau_d \approx 30 \text{ min}$. Therefore, under suitable conditions, ideal M-I waves may move a significant distance before they disappear and strongly inertial M-I waves may exist for several hundreds of periods.

8.2. Observations

[90] M-I waves couple two regions of space, so it should be possible to observe them both in the magnetosphere (as inertial AW signatures with particular properties) and in the ionosphere (using radars or optical observations of auroras). Estimates of the typical properties of M-I waves (see section 8.1) suggest that M-I waves are likely to be best observed at night and in regions of suppressed E-region number density. They also require the presence of a transverse electric field, which suggests active auroral regions are a good place to begin looking for M-I waves.

[91] It is likely that one group of existing observations has already detected M-I waves. In recent decades, satellites have observed a class of Alfvén wave whose origin has defied explanation in terms of either the magnetosphere or ionosphere alone. These waves typically occur at the boundary between a large scale pair of upward and downward field-aligned current channels (of the sort commonly associated with the plasma sheet boundary-layer), and appear as intense, short-wavelength electromagnetic disturbances, just inside the downward current channel. They have been observed with the Polar [Keiling *et al.*, 2005], FAST [Paschmann *et al.*, 2002] and Cluster satellites [Karlsson *et al.*, 2004; Wright *et al.*, 2008]. Since Cluster is a constellation of four spacecraft, it has been possible to separate spatial and temporal variation in these data and the typical period of these waves has been estimated as about 20–40 seconds [Karlsson *et al.*, 2004].

[92] The period of these waves is too long for a traditional ionospheric explanation such as trapping inside an ionospheric Alfvén resonator and the waves have been observed at an altitude of 4–7 R_E which is well above any ionospheric trapping region. On the other hand, the period is much shorter than typical magnetospheric timescales (such as the Alfvén wave transit time along field-lines). Thus, attempts to match the period of these waves with natural periods of either the magnetosphere or ionosphere (in isolation) have been unsuccessful.

[93] One promising line of research has been the hypothesis that narrow scale waves are generated by a nonlinear interaction of large scale FACs (created by magnetospheric processes) with an active ionosphere. A series of numerical studies by *Streltsov and Lotko* [2004, 2005] and *Streltsov and Karlsson* [2008] have firmly established that intense narrow-scale waves are indeed produced at the boundary between upward and downward current channels by the interaction between magnetosphere and ionosphere, and the simulated waves bear a strong resemblance to observations. Some of those numerical studies use the same governing equations as this paper so it is reasonable to assert that the waves in those computer simulations, and hence the waves observed by spacecraft, are M-I waves. This is supported by the observed periods of 20–40 seconds, which agrees well with the M-I wave periods estimated in section 8.1. M-I wave theory is, therefore, the first theory capable of explaining the properties (period and transverse scale) and generation mechanism of this class of Alfvén wave.

[94] M-I waves may also illuminate the study of auroral arcs. When the upward current density associated with an M-I wave passes some threshold, precipitation of magnetospheric electrons will produce auroral arcs. Therefore, M-I waves are likely to have a signature in optical observations of auroras. Arcs that evolve as M-I waves will move in the direction of the transverse electric field, traveling at the M-I wave phase speed. Wavebreaking, in particular, could produce rich auroral behavior: e.g. a wide arc at the leading edge of an M-I wave may broaden and dim while a series of intense, narrow arcs are produced at the trailing edge of the wave. This would be similar to auroral breakup as observed by *Semeter et al.* [2008].

8.3. Opportunities for Experimental Verification

[95] Many of the results given in this paper can be tested, for example, by using ionospheric heaters of the type available through HAARP and EISCAT to modify E-region plasma density at a time when a horizontal electric field is present in the ionosphere. The ionospheric disturbances produced by these heaters ought to show features distinctive of M-I waves.

[96] The best conditions for such experiments are low background number density so that M-I waves have a long lifetime, and a strong transverse electric field so that M-I waves evolve significantly during their lifetime. These conditions naturally occur at night in the downward return current region adjacent to visible auroral arcs, which are the same conditions favored by IFI experiments [*Streltsov et al.*, 2010].

[97] Since M-I wave theory is most developed for 1D perturbations in E-region plasma density, it would be desirable to create a perturbation that is extended in the $\mathbf{E} \times \mathbf{B}$ direction. This approach would test the 1D results presented in the first part of this paper and could be achieved either by shaping the radar beam or by sweeping it back and forth rapidly over a region of sky. Such studies would likely concentrate first on ideal M-I waves since these do not require a tight focus of the heater’s radar beam. Several modes of heater operation can be imagined. The simplest test would verify that M-I waves move in the direction of the transverse electric field: if the heater is constantly on at a fixed location, then we expect a change in E-region plasma

density there, and advection will subsequently produce an asymmetry in the perturbed plasma density, making the perturbation more extended on the ‘downwind’ side. The extended tail so produced will decay with distance from the heated region and should have an e-folding length $\lambda_d = (v_{MI}\tau_d)^{-1}$ (where localized heating makes τ_d a function of position). Further modes of heater operation include pulsed drivers (creating single wave packets or extended wave trains) which should exhibit advection, damping, and (depending on the amplitude) wavebreaking.

[98] Experimental studies would benefit from accompanying or preceding numerical studies that define the expected outcomes for proposed modes of operation. These could easily be performed by modifying simulations like those presented in this paper to make the recombination coefficient, α , a function of position and time. Variations in $\alpha(y, t)$ would then serve as a proxy for the effects of an ionospheric heater. A study of this type has already been performed by *Streltsov and Pedersen* [2010] in a search for effective methods to generate magnetospheric Alfvén waves by ionospheric heating. Those authors observed that E-region density features (produced by heating) move in the direction of the electric field at a characteristic speed, and a stronger system response is produced when the region of ionospheric heating itself moves at this speed. Recent correspondence with these authors has established that the characteristic speed noted in their simulations (74.3 ms^{-1}) agrees with the advection speed v_{MI} derived in this paper. There is some flexibility in the choice of ideal Σ_A used to calculate v_{MI} for these simulations but exact agreement is obtained using a value of v_A from close to the Alfvén speed minimum above the E-region. This is in keeping with the expectation that M-I wave properties are determined by magnetospheric conditions immediately above the E-region. Although *Streltsov and Pedersen* [2010] were unaware of the M-I wave results presented in this paper, we consider their paper a good illustration of the importance and usefulness of M-I wave theory.

9. Summary and Conclusion

[99] This paper has identified the existence of M-I waves as a consequence of self-consistent electrodynamic M-I coupling and derived simple formulas for their properties. The principle findings are as follows:

[100] 1. Large scale (ideal) disturbances, for which electron inertia is unimportant, move in the direction of the electric field at a characteristic advection speed given in section 8.1.1. This may be as fast as several hundred meters per second or half the $\mathbf{E} \times \mathbf{B}$ speed. Previous works [e.g., *Sato*, 1978; *Miura and Sato*, 1980; *Lysak*, 1991] have considered linear normal modes and related auroral arc motion to phase speed. We have expanded this idea by stressing the importance of both group and phase velocities, relating these to the intuitive and valuable concept of advection, and providing a simple formula for the advection speed.

[101] 2. Advection of large scale waves is nonlinear because the M-I advection speed depends on height-integrated E-region plasma density (equivalently height-integrated Pedersen conductivity). This leads to wavebreaking: M-I waves steepen on their trailing edge, rapidly generating narrow horizontal length scales. Wavebreaking is a new mechanism

for production of narrow length scales in the ionosphere and magnetosphere. This mechanism does not rely on magnetospheric trapping, so it is able to operate independently of IFI; it may also be faster than phase-mixing. Steepening of waveforms has been observed before in IFI simulations [e.g., *Lysak and Song, 2002*] and our analysis offers detailed insight into the steepening process, and explains where steepening occurs.

[102] 3. M-I waves with electron inertial scales ($\lambda_{\perp} \lesssim 2\pi\lambda_e$) behave very differently to their ideal counterparts. We have shown that group and phase velocities of inertial M-I waves are always slower than the ideal advection speed. As $\lambda_{\perp}/\lambda_e$ is decreased, M-I waves become progressively slower, until in the strongly inertial limit ($\lambda_{\perp} \lesssim \lambda_e$) the group velocity goes to zero and M-I waves oscillate at a characteristic frequency given in section 8.1.2. This characteristic frequency is also an upper limit on the frequency of M-I waves, estimates of which give periods from several tenths of a second to several minutes, depending on magnetospheric and ionospheric conditions.

[103] 4. Wavebreaking of a large-scale M-I wave packet produces a wake of electron inertial scale waves, which trails behind the initial steepening. The largest wavelength so produced is defined by the scale at which dispersive effects noticeably reduce the normal-mode group speed below the ideal advection speed, allowing separation from the main wave packet: this is approximately $2\pi\lambda_e$. Further along the electron inertial train, the length scale becomes smaller because the smallest wavelengths have the smallest group speeds and therefore become most separated from the main wave packet. A combination of wavebreaking and dispersion can therefore populate the M-I system with many electron-inertial scale features.

[104] 5. M-I waves are closely linked to other self-consistent M-I coupling phenomena such as ionospheric feedback instability. Here, we have used the convenient formulas of M-I waves to provide new insight into the overreflection that energizes IFI, showing that downgoing Alfvén waves are best amplified by reflection from the E-region when their phase speed matches the phase speed of an M-I wave with the same spatial scale. M-I wave properties therefore define the phase speed of the most unstable modes for IFI, while the eigenmodes of IAR (or reflection from a conjugate ionosphere) defines the frequency of these modes. It has been known for some time that growth of IFI, for a given frequency, is strongest for a certain spatial scale; resonance of phase-speed to a ‘natural’ M-I phase-speed gives a reason why this should be so.

[105] Further to the above, we have also used IFI results to obtain a dispersion relation for 2D M-I waves. The 2D dispersion relation suggests that the properties of M-I waves identified in 1D also carry over to 2D. There are some modifications to the advection speed and characteristic frequency of oscillation and these are discussed in section 7. Further studies should be done to confirm these expectations.

[106] A complete understanding of the coupled M-I system ultimately requires a range of models using complementary levels of physical detail: more tractable models are useful for isolating and studying individual processes, whereas more complex models provide realism. The present work has focused on local aspects of dynamic M-I coupling and so

falls at the simpler end of this spectrum. Similarly, much IFI theory has also emphasized tractable models, e.g. through the study of linear normal-modes or by modeling magnetospheric trapping through a modified Alfvén conductance, as done by *Sato [1978]* and *Lysak [1991]*. In contrast, numerical simulations of M-I coupling [e.g., *Streltsov and Lotko, 2004*] are capable of highly realistic modeling, but their interpretation can be difficult. One of the next steps to close the gap between realism and understanding is to revisit simulations of M-I wave packets with realistic variation of Alfvén speed (and hence magnetospheric trapping), of the type performed by *Lysak and Song [2002]*. M-I wave theory offers several new insights (e.g. nonlinear M-I advection) and this is an excellent scenario in which to study IFI for waves that are not linear normal modes. It will also be interesting to improve magnetospheric modeling to include nonlinear effects: studies of geomagnetic field line resonances by *Lu et al. [2003]* and *Prakash et al. [2003]* have shown that nonlinear effects can interact with dispersive terms to produce short length scales parallel to the magnetic field; such effects may play a similar role for M-I waves also.

[107] M-I waves couple two regions of space, so it should be possible to observe them both in the magnetosphere and in the ionosphere. Recombination damps M-I waves, suggesting they are to be best observed at night and in regions of low E-region plasma-density. The waves also require the presence of a transverse electric field, which suggests active auroral regions are a good place to begin looking for them. A search to confirm the existence of and properties of M-I waves could look for naturally occurring waves, or use ionospheric heaters to excite them. We also draw attention to satellite [*Keiling et al., 2005; Paschmann et al., 2002; Karlsson et al., 2004; Wright et al., 2008*] and auroral [*Semeter et al., 2008*] observations that show many of the expected properties of M-I waves.

[108] The theory of M-I waves not only improves our understanding of our planet, it also encourages development of applications, for example in M-I diagnostics and space-situational awareness. The advection speed and characteristic frequencies have simple dependencies on ionospheric and magnetospheric parameters. They could therefore be used to constrain our knowledge of the M-I system at any given time, either by passive observation of naturally occurring M-I waves, or by using ionospheric heaters to create them. Wavebreaking of man-made M-I waves (together with IFI) could potentially be used to populate the F-region with small-scale waves to improve the signal returned to incoherent scatter radars. It is also desirable for mankind to develop a capability for efficiently exciting Alfvén waves in the magnetosphere as a means of modifying our immediate space environment (e.g. by using wave-particle interactions to scatter energetic particles out of Earth’s radiation belt). M-I wave theory provides frequencies and velocities for which the coupled M-I system cooperates with this purpose.

[109] **Acknowledgments.** The authors are grateful to the International Space Science Institute (Switzerland) for funding the program that inspired this work, and to Anatoly Streltsov for leading that program. AJBR acknowledges an STFC studentship that funded the majority of this work and is grateful to the Royal Commission for the Exhibition of 1851 for present support.

[110] Robert Lysak thanks the reviewers for their assistance in evaluating this paper.

References

- Atkinson, G. (1970), Auroral arcs: Result of the interaction of a dynamic magnetosphere with the ionosphere, *J. Geophys. Res.*, *75*, 4746–4755, doi:10.1029/JA075i025p04746.
- Bilitza, D. (2001), IRI 2000, *Radio Sci.*, *36*, 261–276, doi:10.1029/2000RS002432.
- Cran-McGreehin, A. P., A. N. Wright, and A. W. Hood (2007), Ionospheric depletion in auroral downward currents, *J. Geophys. Res.*, *112*, A10309, doi:10.1029/2007JA012350.
- Holzer, T. E., and T. Sato (1973), Quiet auroral arcs and electrodynamic coupling between the ionosphere and the magnetosphere, *2, J. Geophys. Res.*, *78*, 7330–7339, doi:10.1029/JA078i031p07330.
- Karlsson, T., G. Marklund, S. Figueiredo, T. Johansson, and S. Buchert (2004), Separating spatial and temporal variations in auroral electric and magnetic fields by Cluster multipoint measurements, *Ann. Geophys.*, *22*, 2463–2472.
- Keiling, A., G. K. Parks, J. R. Wygant, J. Dombek, F. S. Mozer, C. T. Russell, A. V. Streltsov, and W. Lotko (2005), Some properties of Alfvén waves: Observations in the tail lobes and the plasma sheet boundary layer, *J. Geophys. Res.*, *110*, A10S11, doi:10.1029/2004JA010907.
- Lu, J. Y., R. Rankin, R. Marchand, and V. T. Tikhonchuk (2003), Nonlinear acceleration of dispersive effects in field line resonances, *Geophys. Res. Lett.*, *30*(10), 1540, doi:10.1029/2003GL016929.
- Lysak, R. L. (1991), Feedback instability of the ionospheric resonant cavity, *J. Geophys. Res.*, *96*, 1553–1568, doi:10.1029/90JA02154.
- Lysak, R. L., and Y. Song (2002), Energetics of the ionospheric feedback interaction, *J. Geophys. Res.*, *107*(A8), 1160, doi:10.1029/2001JA000308.
- Mann, I. R., A. N. Wright, K. J. Mills, and V. M. Nakariakov (1999), Excitation of magnetospheric waveguide modes by magnetosheath flows, *J. Geophys. Res.*, *104*, 333–354, doi:10.1029/1998JA900026.
- Mills, K. J., and A. N. Wright (1999), Azimuthal phase speeds of field line resonances driven by Kelvin-Helmholtz unstable waveguide modes, *J. Geophys. Res.*, *104*, 22,667–22,678, doi:10.1029/1999JA900280.
- Miura, A., and T. Sato (1980), Numerical simulation of global formation of auroral arcs, *J. Geophys. Res.*, *85*, 73–91, doi:10.1029/JA085iA01p00073.
- Ofman, L., M. Balikhin, C. T. Russell, and M. Gedalin (2009), Collisionless relaxation of ion distributions downstream of laminar quasi-perpendicular shocks, *J. Geophys. Res.*, *114*, A09106, doi:10.1029/2009JA014365.
- Paschmann, G., S. Haaland, and R. Treumann (Eds.) (2002), *Auroral Plasma Physics, Space Sci. Rev.*, *103*, doi:10.1023/A:1023088315789.
- Prakash, M., R. Rankin, and V. T. Tikhonchuk (2003), Precipitation and nonlinear effects in geomagnetic field line resonances, *J. Geophys. Res.*, *108*(A4), 8014, doi:10.1029/2002JA009383.
- Russell, A. J. B. (2010), Coupling of the solar wind, magnetosphere and ionosphere by MHD waves, Ph.D. thesis, Univ. of St Andrews, St Andrews, UK.
- Russell, A. J. B., A. N. Wright, and A. W. Hood (2010), Self-consistent ionospheric plasma density modifications by field-aligned currents: Steady state solutions, *J. Geophys. Res.*, *115*, A04216, doi:10.1029/2009JA014836.
- Sato, T. (1978), A theory of quiet auroral arcs, *J. Geophys. Res.*, *83*, 1042–1048, doi:10.1029/JA083iA03p01042.
- Semeter, J., M. Zettergren, M. Diaz, and S. Mende (2008), Wave dispersion and the discrete aurora: New constraints derived from high-speed imagery, *J. Geophys. Res.*, *113*, A12208, doi:10.1029/2008JA013122.
- Streltsov, A. V., and T. Karlsson (2008), Small-scale, localized electromagnetic waves observed by Cluster: Result of magnetosphere-ionosphere interactions, *Geophys. Res. Lett.*, *35*, L22107, doi:10.1029/2008GL035956.
- Streltsov, A. V., and W. Lotko (2004), Multiscale electrodynamic of the ionosphere-magnetosphere system, *J. Geophys. Res.*, *109*, A09214, doi:10.1029/2004JA010457.
- Streltsov, A. V., and W. Lotko (2005), Ultra-low-frequency electrodynamic of the magnetosphere-ionosphere interaction, *J. Geophys. Res.*, *110*, A08203, doi:10.1029/2004JA010764.
- Streltsov, A. V., and T. R. Pedersen (2010), An alternative method for generation of ULF waves by ionospheric heating, *Geophys. Res. Lett.*, *37*, L14101, doi:10.1029/2010GL043543.
- Streltsov, A. V., T. R. Pedersen, E. V. Mishin, and A. L. Snyder (2010), Ionospheric feedback instability and substorm development, *J. Geophys. Res.*, *115*, A07205, doi:10.1029/2009JA014961.
- Wright, A. N., C. J. Owen, C. C. Chaston, and M. W. Dunlop (2008), Downward current electron beam observed by Cluster and FAST, *J. Geophys. Res.*, *113*, A06202, doi:10.1029/2007JA012643.

A. J. B. Russell, School of Physics and Astronomy, University of Glasgow, Kelvin Building, Glasgow G12 8QQ, UK. (alexander.russell@glasgow.ac.uk)

A. N. Wright, School of Mathematics and Statistics, University of St Andrews, North Haugh, St Andrews KY16 9SS, UK. (andy@mcs.st-andrews.ac.uk)